

Dual Frequency Branch Framework with Reconstructed Sliding Windows Attention for AI-Generated Image Detection

Jiazhen Yan, Ziqiang Li, Fan Wang, Ziwen He, Zhangjie Fu, *Member, IEEE*,

Abstract—The rapid advancement of Generative Adversarial Networks (GANs) and diffusion models has enabled the creation of highly realistic synthetic images, presenting significant societal risks, such as misinformation and deception. As a result, detecting AI-generated images has emerged as a critical challenge. Existing researches emphasize extracting fine-grained features to enhance detector generalization, yet they often lack consideration for the importance and interdependencies of internal elements within local regions and are limited to a single frequency domain, hindering the capture of general forgery traces. To overcome the aforementioned limitations, we first utilize a sliding window to restrict the attention mechanism to a local window, and reconstruct the features within the window to model the relationships between neighboring internal elements within the local region. Then, we design a dual frequency domain branch framework consisting of four frequency domain subbands of DWT and the phase part of FFT to enrich the extraction of local forgery features from different perspectives. Through feature enrichment of dual frequency domain branches and fine-grained feature extraction of reconstruction sliding window attention, our method achieves superior generalization detection capabilities on both GAN and diffusion model-based generative images. Evaluated on diverse datasets comprising images from 65 distinct generative models, our approach achieves a 2.13% improvement in detection accuracy over state-of-the-art methods.

Index Terms—Deepfake detection, AI-generated image detection, AI security, Window attention.

I. INTRODUCTION

WITH the rapid advancement of deep learning, generative models such as GANs and diffusion models have revolutionized content creation, finding widespread applications across industries including entertainment and media. However, this progress has also introduced significant challenges. The increasing sophistication of deepfake technology has allowed the generation of highly realistic fake images and videos, making them increasingly difficult to detect and posing serious risks to societal trust, individual privacy, and security.

To prevent the abuse of generative methods, a series of AI-generated image detection mechanisms have been conceived. Early methods primarily focused on analyzing image features, such as texture, color, and lighting [1, 2] to identify forgery traces. However, these methods are usually limited to the domain consistent scenario, where the training and testing

sets come from the same type of generative method, resulting in poor generalized detection performance in cross-generative method scenarios. With the continuous deepening of research, it is widely recognized that artifacts are often confined to subtle and localized areas. Inspired by this, extensive research has been conducted to extract generalizable and fine-grained forgery features. Specifically, Tan *et al.* [3] extracted more generalized artifact information from the generator's perspective by analyzing the relationship between adjacent pixels. Other works [4–6] have further amplified the local artifacts by means of segmenting patches, thus achieving better detection performance. In addition, some studies [7–9] captured forgery traces from the perspective of frequency domain to obtain more generalized detection performance.

Although extracting local features has been widely adopted to capture generalized forgery artifacts, there are still some deficiencies as follow. 1) The existing works all lack consideration of the importance differences and interdependencies of internal elements of local regions. Although the common attention mechanism [10–12] can adaptively assign different weights to different local regions, they are not sensitive enough to the importance and interrelationship among the internal elements within the local regions. 2) Most existing works are limited to extracting local artifact features in a single frequency domain, resulting in the extracted features being insufficient for precisely capturing the general forgery traces caused by diverse generation methods.

To address above issues, it is urgent for the proposed method to tackle the following two difficulties. **1) How to model the importance difference and complex dependencies of elements within local regions?** we adopt a sliding window to limit the attention mechanism to a local window and reconstruct the features within the window, making the attention mechanism more adaptively focused on pixel-level details while retaining the complex dependencies between pixels. Specifically, we concatenate features from the different frequency bands in each frequency domain. Then the nearby features are tiled in each frequency band. Finally, a sliding window is applied to extract the tiled features from all frequency bands. In this way, the reconstructed window features not only obtain features from the different frequency bands, but also retain the implicit relationships between adjacent elements. **2) How to extract more abundant and effective local features to further amplify the forgery traces?** It is well known that the DWT domain can reflect local spatial frequency features containing high-frequency and low-frequency texture information [13–15]. In this paper, we find that each element of the phase part in the FFT domain contains the dependencies and structural relationship between the overall elements. That

This work was supported in part by the National Natural Science Foundation of China under grant U22B2062, 62172232, 62202233, 62172234, by the China Postdoctoral Science Foundation numbers 2023M741778. (Corresponding author: Zhangjie Fu).

Jiazhen Yan, Ziqiang Li, Fan Wang, Ziwen He and Zhangjie Fu are with the Engineering Research Center of Digital Forensics, Ministry of Education, Nanjing University of Information Science and Technology, Nanjing, 210044, China. (e-mail: 247918horizon@gmail.com, iceli@mail.ustc.edu.cn, wf711103@126.com, {ziwen.he, fzj}@nuist.edu.cn).

means it can capture the longer-range dependencies between the global elements, thereby enriching the extracted fine-grained local features from another perspective. To verify the rationality of above finding, we randomly selected 1k real images and 1k fake images from the dataset GenImage, and cropped them to the same size. We randomly exchange the phase part of the real image and the fake image, and use the swapped images as the input of the detector. The average prediction results of the images predicted as fake are shown in Figure 1. The smaller the prediction result is, the more likely the image is to be classified as a real image. We find that the detector tends to judge images with fake phase as fake category rather than fake amplitude. This indicates that the phase part contains more artifact traces. Moreover, the amplitude part mainly contains properties such as color and brightness, which is difficult to reflect forgery traces, as described in [16].

Therefore, we design a dual frequency branch framework consisting of four frequency bands in the DWT domain and the phase part in the FFT domain to extract richer local artifact features from multiple perspectives. Based on this, a reconstructed sliding window attention mechanism is designed to obtain more fine-grained and generalized local artifact features, thus improving the detection performance across various generation methods. To fully assess the generalizability of our method, we evaluate it on large image datasets generated by 65 distinct generation models¹. Comprehensive experimental results show that our method achieves a significant improvement over state-of-the-art methods C2P_CLIP [17] and AIDE [18] by 5.8% and 7.0%. The overall contributions of the proposed method can be summarized as follows.

- We creatively reconstructed the sliding window attention mechanism, which effectively constructs the features within the window while limiting the attention within the local window, so that the attention mechanism can more accurately measure the importance and interdependence between internal elements in the local area.
- We discovered that the phase part of FFT domain can reflect the artifact traces precisely in addition to the high and low frequency information of the DWT domain, and further designed the dual frequency branch framework to extract richer local forgery features from multiple perspectives.
- Comprehensive experimental results have verified that our method exhibits strong generalization ability across 65 different generative methods. Compared with the state-of-the-art methods, the detection accuracy is improved by 2.13%, which further highlights its superiority and universality.

¹AtGAN, BEGAN, CramerGAN, InfoMaxGAN, MMDGAN, RelGAN, S3GAN, SNGAN, STGAN, ADM, DDPM, IDDP, LDM, PNDM, VQD-iffusion, SDv1, SDv2, Guided, Glide_50_27, Glide_100_10, Glide_100_27, LDM_100, LDM_200, LDM_200_cfg, DALLÉ, ProGAN, StyleGAN, StyleGAN2, BigGAN, CycleGAN, StarGAN, GauGAN, Deepfake, WFIR, ADM, Glide, Midjourney, SDv1.4, SDv1.5, VQDM, Wukong, DALLÉ2, R3GAN, StyleGAN3, StyleGAN-XL, StyleSwim, BlendFace, E4S, FaceSwap, InSwap, SimSwap, FLUX1-dev, Midjourney V6, GLIDE, DALLÉ-3, Imagen3, SD3, SDXL, BLIP, Infinite-ID, InstantID, IP-adaptor, PhotoMaker, SocialRF, CommunityAI

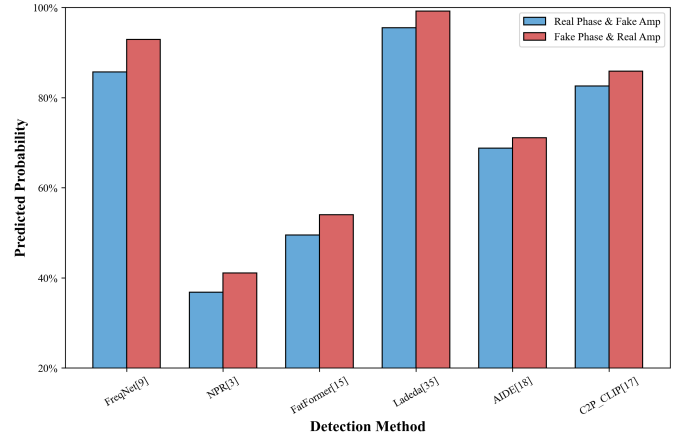


Fig. 1: **Average Prediction Results of the Exchange Phase.** The smaller the predicted number, the more likely the model is to classify the image as real. The detector consistently judged the images with false phase as false images rather than the images with false amplitude.

II. RELATED WORK

With the continuous development of generation methods, including GAN[19–22], diffusion [23–26], customized generation [27–31] and so on, the generated images are becoming more and more realistic, and the naked eye can no longer distinguish the authenticity of the images. In order to solve the future brought about by the above problems, many researchers are committed to the detection of AI-generated images. In this section, we will briefly introduce the existing detection methods from two aspects.

A. Exploration of Fine-Grained Features in AI-Generated Image Detection

Early researches on AI-generated image detection often focused on specific facial regions, such as the eyes and lips, to identify forgery traces [32, 33]. However, as forgery techniques have advanced, these simple traces have been increasingly refined and obscured, rendering biometric-based detection methods insufficient for identifying sophisticated forgery images. Experiments show that forgery traces are often embedded in fine details, which motivates people to turn to extracting local artifact information, including spatial and frequency domains. In terms of spatial domains, some researches narrow the focus to local areas to extract artifact information, including limited receptive fields [34, 35], cropping the image into smaller patches [4–6, 36], etc. Specifically, Chai *et al.* [34] employ limited receptive fields to identify patches that render images detectable, Zheng *et al.* [6] divides the image into multiple patches and shuffles them, and trains a block-based convolutional network for feature extraction. In addition, LGrad [8] employs pretrained CNN models as transform functions to convert images into gradients and leverages these gradients to present universal artifacts. NPR [3] improve generalization by identifying upsampling artifacts, such as pixel grid distortions, in nearby regions. In the frequency domain, F3-Net [37] introduces frequency component division and the frequency statistical difference

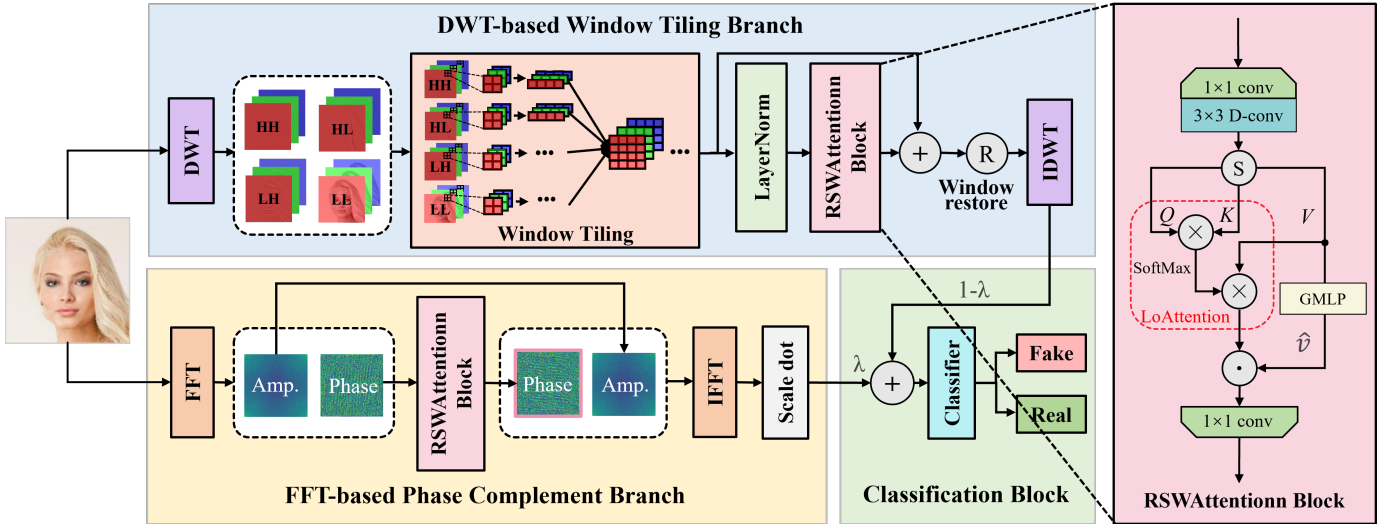


Fig. 2: **Architecture of Our Method for Generalizable AI-Generated Image Detection.** Specifically, we first design a reconstructed sliding window attention mechanism, which reconstructs the features within the sliding window and limits the attention mechanism to the local window range, forcing the attention to extract fine-grained forgery features while modeling the importance and dependencies between internal elements in the local area. At the same time, we designed a dual frequency branch framework, which facilitates the model to extract richer artifact traces from multiple perspectives by using DWT-based window tiling and the phase part of FFT. The final extracted features are passed into a classifier.

between real images and forgery images into face forgery detection. FreDect [38] observes significant artifacts in the frequency domain of GAN-generated images, attributed to the upsampling operation in GAN architectures. Luo *et al.* [39] utilize multiple high-frequency features of images to enhance generalization performance. FreqNet [9] utilize the Fast Fourier Transform (FFT) to extract global high-frequency information, revealing refined forgery features such as periodic noise or anomalies invisible in the spatial domain. AIDE [18] improved the generalization ability of forgery detection by extracting the highest and lowest fine-grained patches through DCT to capture low-level fine-grained artifact information.

B. Application of Attention in AI-generated Image Detection

Previous studies [10–12] has proven that: The attention mechanism can not only be trained to focus on important areas of the image, but also capture the long-range dependencies of the image, which is very useful in AI-generated image detection. Many works have explored this: Zhao *et al.* [40] employ multiple spatial attention heads, allowing the model to attend to distinct regions—such as the eyes and mouth—simultaneously, enhancing its ability to spot inconsistencies. Wu *et al.* [41] introduce a local attention module interacting with distant structures (e.g., PPG graphs), though further details from the original study would clarify this mechanism. In recent years, the attention mechanism has been widely integrated into advanced models such as Vision Transformer (ViT) [12] and CLIP [42], which not only improves the accuracy of detection, but also brings new possibilities for dealing with increasingly complex forgery techniques. For example, Ojha *et al.* [43] directly utilizes image features from the CLIP model for linear classification, LASTED [44] proposes designing textual labels to supervise the CLIP vision model through image-text contrastive learning, further advancing the

field of AIGC detection, Fatformer [15] introduces a forgery-aware adapter to discern and integrate local forgery traces based on CLIP. CLIPMoLE [45] adapts a combination of shared and separate LoRAs within an MoE-based structure in deeper ViT blocks. What’s more, C2P_CLIP [17] explored the reasons and potential of CLIP’s effectiveness in AI-generated image detection, and for the first time integrated category common cues into the text encoder to inject category-related concepts into the image encoder, thereby improving detection performance.

Existing attention mechanisms, such as Vision Transformers (ViT) and CLIP, typically capture global weights and long-range dependencies to extract broad semantic information. However, they lack sensitivity to the significance and inter-relationships of elements within local regions, hindering their ability to effectively detect fine-grained forgery traces. Therefore, we propose a reconstructed sliding window attention mechanism, which enhancing the feature extraction capacity of the window attention block to model the importance and dependencies of local forgery features. In addition, a dual frequency branch network is designed to enrich the features within the window from different angles, which promotes the extraction of more comprehensive local forgery features in the window.

III. THE PROPOSED METHOD

A. Main Backbone

The overall structure of our method is shown in Figure 2. Specifically, we first propose a reconstructed sliding window attention mechanism, which reconstructs the features within the window while limiting the attention to the local window, forcing the attention to extract fine-grained forgery traces while modeling the importance and interdependence between

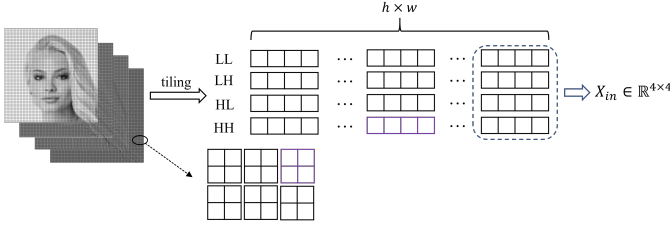


Fig. 3: After DWT, sliding window tiling is used to tile the features of each channel into a shape of $4 \times (h \times w)$. In the subsequent LoAttention module, 4×4 features are extracted as shown in the blue box, which not only obtain features from the different frequency bands, but also retain the implicit relationships between adjacent elements.

internal elements within the local range. In addition, in order to enrich the extraction of local features from different perspectives, we design a dual frequency branch framework, using DWT-based window tiling and phase part of FFT before using window attention. In this way, the window feature not only obtains the features of different frequency bands, but also retains the implicit relationship between adjacent elements, while complementing the long-range dependency between features, which improves the overall generalization ability of the model.

B. Reconstructed Sliding Window Attention Block

The Reconstructed Sliding Window Attention Block (RSWAttention) consists of two main components: (i) the Local Attention Block (LoAttention) and (ii) the Global Window MLP Layer (GMLP). Before feeding the features into LoAttention and GMLP, we preprocess them to enhance their representational quality. A 1×1 convolution layer is applied to extract cross-channel features, following by a 3×3 depthwise separable convolution to better capture the local features within each channel. The resulting convolved features are denoted as $X_{in} \in \mathbb{R}^{B \times C \times H \times W}$.

LoAttention. The attention mechanism obtains better results by training different weights of features. However, the weights of traditional attention mechanisms are derived from the features of the entire image, which contains a lot of semantic information. This weight design may cause the model to be disturbed when extracting fine-grained forgery traces. Thus we designed LoAttention module. Specifically, we employ a sliding window approach that divides the features into windows of size $b \times b$. By restricting the attention module to these local windows, the focus shifts to effectively extracting local features. The features are then divided into $Q, K, V \in \mathbb{R}^{S \times C \times N}$, where $S = B \times \frac{H}{b} \times \frac{W}{b}$ and $N = b \times b$, as required by the attention module. Since the attention operates locally within each window, the features within window i are represented as $Q_i, K_i, V_i \in \mathbb{R}^{C \times N}$. These localized features are fed into the attention module for computation:

$$A_i = \text{Attention}(Q_i, K_i, V_i) = \text{SoftMax}(Q_i K_i^\top) V_i. \quad (1)$$

The results of all sliding window attention operations can be expressed as $A = \{A_1, A_2, \dots, A_S\} \in \mathbb{R}^{S \times C \times N}$.

GMLP. To preserve global correlations while capturing fine-grained features, we integrate a global MLP within each window. This aims to address the limitations of local windows in modeling global relationships, ensuring a seamless fusion of local details and global context. Specifically, we reuse the value V_i from LoAttention and process it through the global MLP, applying a nonlinear transformation to enhance its representational capacity. The result \hat{V}_i is formally expressed as:

$$\text{GMLP}(V_i) = G(\text{Linear}(V_i)), \quad (2)$$

where $G(\cdot)$ denotes the GELU function. The GMLP recombinates and redistributes the local window information, enabling the mixing of local frequency domain features and enhancing the learning of global features.

After combining the outputs from LoAttention and GMLP via a dot product, we use the inverse window operation to restore the feature to its original size $B \times C \times H \times W$, followed by a convolution to map the features back to the original feature dimensions. The final output of the RSWAttention can be expressed as:

$$X_W = \text{conv}(\sum_{i=1}^s \text{Attention}(Q_i, K_i, V_i) \cdot \sum_{i=1}^s G(\text{Linear}(V_i))). \quad (3)$$

C. Dual Frequency Branch Feature Enrichment Module

DWT-based window tiling branch. Previous methods often leverage the Fast Fourier Transform (FFT) or Discrete Cosine Transform (DCT) to capture relationships between adjacent nodes in the frequency domain. However, these approaches can lead to the loss of positional information, which is crucial for extracting detailed features. To overcome this limitation, we utilize the Discrete Wavelet Transform (DWT), which decomposes the image into the spatial-frequency domain, represented as:

$$\text{DWT}(I) = \{I_{LL}, I_{LH}, I_{HL}, I_{HH}\}, \quad (4)$$

where $I_{LL}, I_{LH}, I_{HL}, I_{HH} \in \mathbb{R}^{C \times \frac{H}{2} \times \frac{W}{2}}$ represent the low-frequency component of the input and the high-frequency components in the vertical, horizontal, and diagonal directions, respectively. To obtain more comprehensive information, we fuse the data from the four frequency domains, resulting in new input features $\hat{I} \in \mathbb{R}^{4 \times C \times \frac{H}{2} \times \frac{W}{2}}$. As illustrated in Figure 3, to extract detailed features, we divide each channel's features into 2×2 windows, with each window capturing localized spatial-frequency information within its respective frequency band. Each window is treated as a small square and tiled into rows within each band. This arrangement ensures that features within the 2×2 windows are preserved in a structured format. Then we tile the features in the window here by rows. At this time, the features from each frequency band are tiled into one row in a specific manner, such that the four adjacent feature values correspond to the 2×2 window from the original image. Additionally, as shown in Figure 3, we integrate features from all frequency bands to generate new input features $\hat{I}_{\text{input}} \in \mathbb{R}^{C \times 4 \times \frac{H \times W}{4}}$. To further

TABLE I: Cross-model Accuracy (Acc.) & Average Precision Score (A.P.) Performance on the GANGen-Detection Dataset [9].

Method	BEGAN		SNGAN		CramerGAN		MMDGAN		RelGAN		STGAN		S3GAN		AttGAN		InfoMaxGAN		Mean	
	Acc.	A.P.	Acc.	A.P.	Acc.	A.P.	Acc.	A.P.	Acc.	A.P.	Acc.	A.P.	Acc.	A.P.	Acc.	A.P.	Acc.	A.P.	Acc.	A.P.
CNNDetection	50.2	44.9	62.7	90.4	81.5	97.5	72.9	94.4	53.3	82.1	63.0	92.7	55.2	66.1	51.1	83.7	71.1	94.7	62.3	82.9
Patchfor	97.1	100.0	97.6	99.8	97.8	99.9	97.9	100.0	99.6	100.0	92.7	99.8	66.8	68.8	68.0	92.9	93.6	98.6	90.1	95.4
F3Net	87.1	97.5	51.6	93.6	89.5	99.8	73.7	99.6	98.8	100.0	60.3	99.9	65.4	70.0	85.2	94.8	67.1	83.1	75.4	93.1
GANDetection	67.9	100.0	66.7	90.6	67.8	99.7	67.7	99.3	60.9	86.2	69.6	97.2	69.6	83.5	57.4	75.1	67.6	92.4	66.1	91.6
LGrad	69.9	89.2	78.0	87.4	50.3	50.3	57.5	67.3	89.1	99.1	54.8	68.0	78.5	86.0	68.6	93.8	71.1	82.0	68.6	80.8
CLIPDetection	88.9	96.3	87.7	96.5	89.8	99.1	89.7	99.0	94.0	98.1	82.6	91.5	94.7	98.9	90.0	96.8	87.4	96.5	89.4	97.0
FreqNet	98.8	100.0	85.4	90.4	95.2	98.2	95.2	98.2	100.0	100.0	98.8	100.0	88.3	94.3	89.8	98.8	94.0	97.5	94.0	97.5
NPR	99.6	99.9	93.3	97.3	98.5	98.3	98.5	98.3	99.8	100.0	99.6	100.0	79.8	78.9	92.5	98.6	91.5	97.2	94.8	96.5
FatFormer	99.9	100.0	98.3	99.9	98.4	100.0	98.4	100.0	99.5	100.0	98.8	99.8	99.0	100.0	99.3	100.0	98.4	100.0	98.9	100.0
Ladeda	100.0	100.0	99.0	99.9	97.9	99.9	99.0	99.9	100.0	100.0	99.8	100.0	80.5	84.9	100.0	100.0	98.4	99.9	97.2	98.3
C2P_CLIP	94.9	100.0	98.4	99.9	98.4	100.0	98.4	100.0	92.0	99.8	97.6	99.6	99.0	100.0	90.4	99.8	98.4	100.0	96.4	<u>99.9</u>
AIDE	57.9	79.5	76.1	79.2	82.0	88.1	82.2	88.3	95.2	96.5	92.7	98.1	69.0	78.8	96.6	98.4	80.7	82.8	81.4	87.8
Ours	98.6	99.7	96.8	99.6	98.0	99.7	98.7	99.8	99.0	99.9	99.1	100.0	88.2	91.1	99.0	99.8	97.2	99.7	<u>97.3</u>	98.8

TABLE II: Cross-model Accuracy (Acc.) & Average Precision Score (A.P.) Performance on the DiffusionForensics Dataset[46].

Method	DDPM		VQ-Diffusion		SDv1		ADM		SDv2		IDDP		PNM		LDM		Mean	
	Acc.	A.P.	Acc.	A.P.	Acc.	A.P.	Acc.	A.P.	Acc.	A.P.	Acc.	A.P.	Acc.	A.P.	Acc.	A.P.	Acc.	A.P.
CNNDetection	62.7	76.6	50.0	71.0	38.0	76.7	53.9	71.8	52.0	90.3	50.2	82.7	50.8	90.3	50.4	78.7	51.0	90.3
Patchfor	62.3	97.1	100.0	100.0	90.7	99.8	77.5	93.9	94.8	100.0	50.0	91.6	50.2	99.9	99.5	100.0	78.1	97.8
F3Net	84.7	99.4	100.0	100.0	73.4	97.2	80.9	96.9	99.8	100.0	74.7	98.9	72.8	99.5	100.0	100.0	85.8	99.0
GANDetection	62.3	46.4	51.1	51.2	39.8	65.6	51.1	53.1	50.1	36.9	50.2	63.0	50.6	79.0	51.6	48.1	50.8	55.4
LGrad	99.9	100.0	96.2	100.0	90.4	99.4	86.4	97.5	97.1	100.0	66.1	92.8	69.5	98.5	99.7	100.0	88.2	98.5
CLIPDetection	72.9	78.8	77.7	99.2	59.0	93.0	88.7	98.6	53.3	87.6	73.4	97.1	86.2	99.2	50.7	87.9	70.2	92.5
FreqNet	91.4	99.8	100.0	100.0	63.9	98.1	67.2	91.3	81.8	98.4	59.0	97.3	85.2	99.8	98.9	100.0	80.9	98.1
NPR	99.4	100.0	100.0	100.0	97.1	99.7	88.4	97.9	96.4	100.0	87.5	98.0	97.5	100.0	100.0	100.0	<u>95.8</u>	99.4
FatFormer	67.2	73.5	100.0	100.0	61.7	96.8	70.8	93.4	84.4	98.2	69.3	94.3	99.3	100.0	97.3	100.0	81.2	94.4
Ladeda	98.4	99.9	100.0	100.0	97.1	99.8	83.9	96.9	94.1	100.0	93.9	98.8	93.7	99.9	100.0	100.0	95.1	<u>99.4</u>
C2P_CLIP	73.4	76.2	95.8	99.7	78.9	99.2	68.8	95.3	66.7	94.8	80.7	94.9	84.2	97.2	97.3	99.7	80.7	94.6
AIDE	86.5	92.5	92.1	99.4	91.5	98.6	85.7	94.1	88.6	95.1	87.8	94.8	89.6	97.8	87.4	95.0	88.6	95.9
Ours	99.9	100.0	100.0	100.0	97.5	99.9	96.0	99.8	99.9	100.0	98.5	100.0	99.2	100.0	99.6	100.0	98.8	100.0

enhance the network’s performance, we apply LayerNorm [47], which ensures that the input data remains within a stable range, reduces dependency on initialization, and improves the stability of model training.

The feature \hat{I}_{input} is then fed into RSWAttention with a sliding window size set to $b = 4$. As depicted in Figure 3, within each 4×4 window, the representation includes not only the four adjacent feature values from the original image but also the feature information across four distinct frequency bands. This configuration provides RSWAttention with comprehensive and fine-grained spatial-frequency domain information, enabling more detailed feature extraction. Following this process, we apply the IDWT to reconstruct the features back into spatial domain representations, denoted as $\hat{I}_{\text{DWT_output}}$.

FFT-based phase complement branch. Different from DWT, which captures local spatial frequency features, each element of the phase part in the FFT domain contains the dependencies and structural relationship between the overall elements, which helps the model capture the long-range dependencies between features. In addition, through our experimental analysis, we found that phase encodes finer details, including potential artifacts. Therefore, in order to enrich the extraction of local fine-grained features from another perspective, we only use the phase part of the FFT as another branch input of the RSWAttention, setting the window size to $b = 8$. The amplitude remains unmodified during this process. After training the phase features, we use IFFT to recombine them with the original amplitude, transforming the

features back into the spatial domain. The resulting features are denoted as $\hat{I}_{\text{FFT_output}}$.

Finally, we set a hyperparameter λ to effectively combines the outputs of two branches. The final feature is:

$$\hat{X}_{\text{output}} = (1 - \lambda) * \hat{I}_{\text{DWT_output}} + \lambda * \hat{I}_{\text{FFT_output}}. \quad (5)$$

IV. EXPERIMENTS

To verify the excellent AI-generated image detection performance of our method, we follow the paradigms of [43] and [50], which will be described in detail below.

A. Dataset

Training set. To ensure a consistent basis for comparison, we use the training set of ForenSynths[50]. The training set consists of 20 different categories, each containing 18,000 synthetic images generated using ProGAN, and an equal number of real images from the LSUN dataset. Following the paradigms of [43], we adopt specific 4-class training settings, denoted as (car, cat, chair, horse).

Testing set. In order to comprehensively compare the effectiveness of our proposed method, we select different GAN and diffusion model-based generated datasets for testing, which contain a wide range of real-world images.

- GANGen-Detection [9]: To evaluate more realistic scenarios, we extend our evaluation using 9 additional GAN-generated images. There are 4K test images for each model, with equal numbers of real and fake images.

TABLE III: Cross-model Accuracy (Acc.) & Average Precision Score (A.P.) Performance on the UniversalFakeDetect Dataset [43].

Method	Guided		Glide_50_27		Glide_100_10		Glide_100_27		LDM_100		LDM_200		LDM_200_cfg		DALLE		Mean	
	Acc.	A.P.	Acc.	A.P.	Acc.	A.P.	Acc.	A.P.	Acc.	A.P.	Acc.	A.P.	Acc.	A.P.	Acc.	A.P.	Acc.	A.P.
CNNDetection	54.9	66.6	54.2	76.0	53.3	72.9	53.0	71.3	51.9	63.7	52.0	64.5	51.6	63.1	51.8	61.3	52.8	67.4
Patchfor	74.2	81.4	84.9	98.8	87.3	99.7	82.8	99.1	95.8	99.8	95.6	99.9	94.0	99.8	79.8	99.1	86.8	97.2
F3Net	69.2	70.8	88.5	95.4	88.3	95.4	87.0	94.5	74.1	84.0	73.4	83.3	80.7	89.1	71.6	79.9	79.1	86.5
GANDetection	50.1	51.0	51.7	53.5	51.2	52.6	51.1	51.9	54.7	65.8	54.9	65.9	53.8	58.9	67.2	83.0	54.3	60.1
LGrad	71.8	76.0	91.6	96.0	90.9	95.5	88.5	94.2	95.7	99.3	94.7	99.1	95.1	99.0	89.9	97.8	89.8	94.6
CLIPDetection	69.7	87.6	79.1	99.8	77.9	94.5	78.5	95.3	95.0	99.3	99.0	99.3	74.0	92.5	87.3	97.5	82.6	95.7
FreqNet	67.3	75.7	86.7	96.3	87.9	96.4	84.5	96.0	97.9	99.9	97.5	99.9	97.4	99.9	97.4	99.8	89.6	95.5
NPR	74.0	78.1	97.5	99.5	97.8	99.5	97.4	99.5	98.2	99.6	98.2	99.6	98.0	99.5	90.9	98.1	93.9	96.7
FatFormer	76.1	92.0	94.7	99.4	94.2	99.2	94.4	99.1	98.7	99.9	98.6	99.8	94.9	99.1	98.8	99.8	93.8	98.5
Ladeda	79.8	87.5	98.3	99.8	98.2	99.8	98.5	99.8	98.6	99.9	98.5	99.9	98.0	99.8	83.9	98.5	<u>94.2</u>	98.1
C2P_CLIP	69.1	94.1	95.3	99.8	96.1	99.8	95.3	99.8	99.3	100.0	99.3	100.0	97.3	99.8	98.6	99.1	93.8	<u>99.2</u>
AIDE	80.4	92.6	94.6	98.9	94.7	98.8	94.5	98.8	93.1	98.6	93.0	98.3	93.3	98.6	92.2	98.0	91.9	97.8
Ours	95.2	97.8	98.0	99.9	97.7	99.9	97.2	99.7	99.4	100.0	99.5	100.0	98.9	99.9	85.2	97.1	96.4	99.3

TABLE IV: Cross-model Accuracy (Acc.) & Average Precision Score (A.P.) Performance on the GenImage Datasets [48].

Method	ProGAN		GauGAN		StyleGAN2		BigGAN		StyleGAN		CycleGAN		StarGAN		Deepfake		WFIR	
	Acc.	A.P.	Acc.	A.P.	Acc.	A.P.	Acc.	A.P.	Acc.	A.P.	Acc.	A.P.	Acc.	A.P.	Acc.	A.P.	Acc.	A.P.
CNNDetection	97.9	99.9	66.1	93.5	67.0	97.1	55.9	80.5	70.1	97.0	76.5	91.5	72.9	93.2	51.7	66.5	62.1	89.4
LGrad	99.9	100.0	72.4	79.3	96.0	99.9	82.9	90.7	94.8	99.9	85.3	94.0	99.6	100.0	58.0	67.9	60.5	65.1
CLIPDetection	100.0	100.0	99.7	100.0	75.7	97.8	95.1	99.3	84.4	97.1	98.7	99.8	99.9	99.4	67.4	82.0	64.2	68.7
FreqNet	99.6	100.0	93.4	98.6	88.0	99.5	90.5	96.0	90.2	99.7	95.8	99.6	85.7	99.8	88.9	94.4	48.0	49.6
NPR	99.9	100.0	80.9	83.0	99.6	100.0	84.0	85.6	98.1	99.8	95.2	98.1	99.8	100.0	77.2	76.0	60.7	63.9
FatFormer	99.9	100.0	99.4	100.0	98.8	99.9	99.5	99.9	97.2	99.8	99.3	100.0	99.8	100.0	93.2	98.0	88.2	98.5
Ladeda	100.0	100.0	94.1	100.0	99.9	100.0	82.5	89.5	99.8	100.0	91.1	99.0	76.2	90.3	64.0	92.6	85.7	93.6
C2P_CLIP	100.0	100.0	99.2	100.0	95.6	99.9	99.1	100.0	96.4	99.5	97.3	100.0	99.6	100.0	93.8	98.6	94.8	99.5
AIDE	98.0	99.8	60.2	71.9	97.5	99.6	71.0	82.2	97.4	99.5	86.0	97.1	99.3	100.0	53.7	70.3	90.3	97.0
Ours	99.8	100.0	85.1	96.7	99.9	100.0	87.1	95.1	99.8	100.0	97.9	98.8	94.9	99.2	64.2	71.8	52.2	46.8

Method	ADM		Glide		Midjourney		SDv1.4		SDv1.5		VQDM		Wukong		DALLE2		Mean	
	Acc.	A.P.	Acc.	A.P.	Acc.	A.P.	Acc.	A.P.	Acc.	A.P.	Acc.	A.P.	Acc.	A.P.	Acc.	A.P.	Acc.	A.P.
CNNDetection	52.1	67.8	51.7	67.1	51.7	64.7	50.6	59.2	50.6	59.2	51.5	63.5	50.5	58.5	50.1	49.2	61.3	76.7
LGrad	65.8	70.2	60.6	73.8	64.6	70.3	65.9	68.7	66.3	69.1	67.2	70.6	63.2	65.0	66.9	86.9	65.1	71.8
CLIPDetection	67.6	87.2	61.7	85.5	56.7	74.5	63.1	87.2	62.8	86.3	84.9	96.8	71.2	90.9	49.5	60.2	73.5	83.6
FreqNet	83.3	91.5	81.7	88.9	69.9	79.0	64.3	74.3	64.9	75.5	81.7	89.6	57.7	67.0	55.1	54.6	69.8	77.6
NPR	70.3	74.9	77.0	83.1	76.4	82.4	76.6	82.7	77.8	83.5	74.9	77.4	74.2	77.9	61.9	71.6	81.4	84.7
FatFormer	78.5	91.8	88.1	96.0	56.1	62.8	67.8	81.1	68.1	81.1	86.9	97.0	73.1	85.9	69.7	81.9	86.1	92.6
Ladeda	74.0	84.4	90.6	96.6	86.9	93.5	89.8	95.5	90.6	95.8	76.6	84.5	87.6	93.0	83.0	93.9	86.6	<u>92.8</u>
C2P_CLIP	77.2	95.8	88.5	98.8	59.2	83.0	82.8	97.3	82.8	97.2	87.2	98.4	80.1	95.5	65.1	92.9	<u>88.2</u>	92.6
AIDE	83.1	95.8	85.9	95.3	69.1	78.1	83.2	95.2	82.8	93.9	80.3	92.2	83.5	95.0	86.6	97.6	82.8	91.8
Ours	94.2	97.3	95.2	98.7	94.7	97.8	94.2	97.6	94.5	98.0	96.5	98.3	93.5	96.9	96.8	99.2	90.6	93.6

- DiffusionForensics [46]: To expand the testing scope, we adopt the diffusions dataset of DIRE [46] for evaluation, including ADM [23], DDPM [51], IDDP [52], LDM [24], PNDM [53], VQ-Diffusion [54], Stable Diffusion v1 [24], Stable Diffusion v2 [24]. The real images are sampled from LSUN and ImageNet datasets.
- UniversalFakeDetect [43]: This test set contains images generated from Glide, DALLE-mini [55], LDM [24]. It adopts images of LAION and ImageNet datasets as the real data.
- AIGCDetectBenchmark [48]: This dataset comprehensively includes GAN and diffusion, and introduces some new diffusion generation methods as detection datasets, including ProGAN, StyleGAN, StyleGAN2, BigGAN, CycleGAN, StarGAN, GauGAN, Deepfake, WFIR, Midjourney, SDv1.4, SDv1.5, ADM, GLIDE, Wukong, VQDM, which is a huge challenge for deepfake detection.
- AIGIBench [49]: AIGIBench is the first benchmark to

conduct a comprehensive evaluation of four critical components in the AIGI detection pipeline, and comprehensively simulates state-of-the-art image generation methods, including: (a) GAN-based noise-to-image generation (ProGAN, StyleGAN3, StyleGAN-XL, StyleSwim, R3GAN, and WFIR), (b) Diffusion for text-to-image generation (SD-XL, SD-3, DALLE-3, Midjourney-v6, FLUX.1-dev, Imagen-3, and GLIDE), (c) GANs for deepfake (BlendFace, E4S, FaceSwap, InSwap, and SimSwap), and (d) Diffusion for personalized generation (InstantID [27], Infinite-ID [28], PhotoMaker [29], BLIP-Diffusion [30], and IP-Adapter [31]). It also includes 2 general subsets featuring fake images collected from social media platforms, which called CommunityAI and SocialRF.

B. Implementation Details

We design a lightweight CNN network using convolutional layers and Resnet network as classifiers. The network is trained

TABLE V: Cross-model Accuracy (Acc.) & Average Precision Score (A.P.) Performance on the AIGIBench Datasets [49].

Method	ProGAN		R3GAN		StyleGAN3		StyleGAN-XL		StyleSwim		WFIR		BlendFace		E4S		FaceSwap	
	Acc.	A.P.	Acc.	A.P.	Acc.	A.P.	Acc.	A.P.	Acc.	A.P.	Acc.	A.P.	Acc.	A.P.	Acc.	A.P.	Acc.	A.P.
CNNDetection	97.8	100.0	49.9	48.4	64.0	91.6	49.7	60.0	58.0	88.9	62.1	89.4	49.3	34.2	49.6	35.2	50.0	44.3
LGrad	98.0	99.9	65.6	69.1	59.9	64.3	61.2	62.8	68.1	75.0	55.6	53.1	38.6	39.4	39.2	39.4	28.2	33.3
CLIPDetection	99.5	100.0	93.0	98.6	68.4	79.0	87.1	95.0	94.5	99.3	91.0	97.8	47.2	42.7	72.4	82.5	69.3	79.4
FreqNet	99.3	100.0	62.3	56.8	83.0	92.4	79.8	84.1	80.8	91.8	58.5	48.9	23.3	34.1	25.8	34.7	40.4	43.4
NPR	99.8	100.0	80.8	75.6	84.1	89.4	74.5	75.9	84.7	91.7	77.8	77.0	33.9	33.3	34.0	34.4	41.1	39.5
FatFormer	99.9	100.0	94.4	99.3	91.5	96.9	93.4	98.0	93.9	99.8	88.2	98.5	46.0	44.7	70.0	73.0	77.6	83.4
LaDeDa	100.0	100.0	72.9	69.2	83.7	86.3	82.1	84.2	82.6	86.4	84.5	91.3	28.2	38.0	29.0	42.4	41.2	40.2
C2P_CLIP	100.0	100.0	95.4	99.8	93.8	98.5	94.1	98.1	95.2	100.0	94.8	99.5	55.2	60.5	69.8	76.1	73.5	82.2
AIDE	98.0	99.8	89.0	94.8	79.2	77.8	84.4	87.7	85.2	85.1	90.3	97.0	43.4	43.8	39.4	38.3	46.7	43.7
Ours	99.8	100.0	94.6	94.9	93.2	98.2	82.3	86.4	94.7	98.6	52.2	46.8	44.1	44.0	45.1	46.4	50.8	66.8

Method	InSwap		SimSwap		FLUX1-dev		Midjourney V6		GLIDE		DALLE-3		Imagen3		SD3		SDXL	
	Acc.	A.P.	Acc.	A.P.	Acc.	A.P.	Acc.	A.P.	Acc.	A.P.	Acc.	A.P.	Acc.	A.P.	Acc.	A.P.	Acc.	A.P.
CNNDetection	50.1	44.3	49.7	45.3	50.3	50.3	49.9	39.3	51.5	67.3	50.4	53.8	51.0	50.3	52.8	66.3	52.6	65.5
LGrad	37.7	38.5	36.1	38.1	64.6	70.0	59.2	62.1	56.7	66.2	49.5	48.6	61.4	66.9	66.2	71.4	64.0	66.3
CLIPDetection	48.9	48.2	50.1	51.5	46.3	39.6	44.8	35.6	69.4	81.7	46.8	38.4	48.1	44.1	49.0	48.6	50.7	53.6
FreqNet	37.5	42.1	36.5	41.9	78.5	87.3	57.6	57.7	75.8	77.4	66.2	61.0	73.6	80.7	77.6	84.0	86.4	93.6
NPR	41.0	36.9	40.5	38.5	87.2	93.6	69.7	71.1	78.2	85.2	57.6	61.9	84.6	91.0	86.4	93.5	87.0	93.7
FatFormer	57.9	66.4	61.7	72.2	48.3	41.8	47.6	43.5	84.5	92.2	50.1	46.8	46.9	43.1	62.9	68.5	75.0	83.0
LaDeDa	38.3	41.8	37.3	39.6	84.2	88.0	67.0	68.0	86.4	89.4	39.2	46.3	81.1	84.6	83.6	87.6	83.1	88.0
C2P_CLIP	59.5	69.0	67.9	78.5	47.6	46.8	51.2	50.2	85.1	93.4	64.4	75.4	45.2	46.5	53.5	65.6	59.3	76.0
AIDE	46.1	43.0	47.2	46.8	84.9	86.6	77.9	78.1	90.0	89.3	56.9	57.0	86.4	90.8	89.7	94.1	88.9	90.0
Ours	52.1	63.7	48.4	57.7	93.2	96.8	86.4	92.7	94.2	98.4	46.2	49.0	93.6	96.0	95.4	97.6	95.9	98.7

Method	BLIP		Infinite-ID		InstantID		IP-Adapter		PhotoMaker		SocialRF		CommunityAI		Mean	
	Acc.	A.P.	Acc.	A.P.	Acc.	A.P.	Acc.	A.P.	Acc.	A.P.	Acc.	A.P.	Acc.	A.P.	Acc.	A.P.
CNNDetection	49.8	44.7	50.8	55.8	50.1	67.1	50.0	50.1	49.6	51.5	50.3	46.3	49.9	50.5	53.6	57.6
LGrad	56.4	57.8	31.3	34.4	53.9	54.8	45.5	46.3	32.0	35.8	49.6	49.3	56.4	63.0	53.4	56.2
CLIPDetection	57.8	68.9	72.4	84.2	67.4	79.5	62.3	73.9	47.0	41.4	49.2	46.2	49.9	50.0	63.3	66.4
FreqNet	93.8	99.9	79.0	74.5	79.8	86.3	78.8	79.9	77.0	74.9	54.2	58.1	55.9	69.7	60.2	61.7
NPR	94.0	97.0	62.0	62.8	71.3	75.9	79.0	81.1	46.4	52.0	54.5	58.4	54.4	60.0	68.2	70.8
FatFormer	82.8	92.3	83.3	91.2	69.3	77.4	67.1	74.1	46.4	37.4	56.9	65.1	51.9	69.9	69.9	74.3
LaDeDa	93.4	96.7	79.0	67.5	81.0	81.8	82.3	82.2	69.3	66.6	56.2	61.7	54.8	55.9	68.8	71.3
C2P_CLIP	84.9	93.8	85.2	93.4	86.8	93.9	55.1	65.9	50.6	52.0	56.4	62.3	51.0	54.5	71.0	77.3
AIDE	92.7	96.7	88.9	87.9	87.6	89.0	87.1	91.0	83.4	80.9	56.8	62.1	51.3	52.8	74.9	76.2
Ours	99.2	99.7	90.0	91.0	94.6	97.7	93.3	96.6	92.7	95.2	60.8	70.8	54.6	66.6	77.9	82.0

using the Adam optimizer[56] with a learning rate of 2×10^{-4} . The batchsize is set to 128, and we train the network for 90 epochs. We also use a learning rate decay strategy that reduces the learning rate by twenty percent after every ten epochs. What's more, the hyperparameter λ is set to 0.4. For the loss function, we used BCELoss, which is commonly used in classification tasks. Our approach is implemented using PyTorch on an NVIDIA RTX A6000 GPU. To evaluate the performance of the proposed method, we follow the evaluation metrics used in baselines [9, 43], which include average precision score (A.P.) and accuracy (Acc.).

C. Quantitative analysis

We compare with the previous methods: CNNDetection [50], Patchfor [34], F3Net [37], FrePGAN [7], GANDetection [57], LGrad [8], CLIPDetection [43], FreqNet [9], NPR [3], FatFormer [15], Ladedda [35], C2P_CLIP [17], AIDE [18]. We conduct comprehensive experiments on five datasets to verify the effectiveness of our method. Specifically, the results of Patchfor [34], F3Net [37], FrePGAN [7], GANDetection [57] all come from NPR [3], and we obtain results of FatFormer

[15], C2P_CLIP [17] using the official pre-trained model. In addition, we retrain all other methods following the paradigms of [43], which adopts specific 4-class training settings, denoted as (car, cat, chair, horse).

GANGen-Detection[9]. Since our method uses ProGAN for training, we first perform cross-domain testing on GAN. As shown in Table I, our detection on GAN has achieved good results. Specifically, it achieves mean Accuracy (Acc.) and mean Average Precision (A.P.) of 97.3% and 98.8%, respectively. Compared to Ladedda and C2P_CLIP, our method improves mean Acc. by 0.1% and 0.9%, respectively. However, on FatFormer, the accuracy is 1.1% higher than our method, which needs to be improved.

DiffusionForensics [46] & UniversalFakeDetect [43]. To further evaluate the generalization ability of our method, we train on ProGAN and test on images generated by various diffusion models. The results are presented in Tables II and III. Despite being trained exclusively on ProGAN-generated images, our method demonstrates strong generalization capabilities across diverse diffusion models. Specifically, it achieves mean Accuracy (Acc.) and mean Average Precision (A.P.) of 98.8% and 100.0%, respectively. Compared with the best

TABLE VI: Module Ablation Studies on the Five Datasets.

DWT	Window Tiling	FFT	RSWAttention	GANGen-Detection	DiffusionForensics	UniversalFakeDetect	GenImage	AIGIBench	mean Acc. / A.P.
✗	✗	✓	✓	49.6 / 49.6	48.6 / 48.6	47.9 / 47.9	49.4 / 49.4	49.6 / 49.6	49.0 / 49.0
✓	✗	✗	✓	93.2 / 96.5	95.6 / 100.0	93.2 / 95.3	87.5 / 91.2	74.1 / 78.5	88.7 / 91.2
✓	✓	✗	✓	95.2 / 97.1	96.9 / 100.0	95.0 / 97.4	88.7 / 92.5	75.5 / 79.8	90.3 / <u>93.4</u>
✓	✗	✓	✓	96.2 / 98.8	96.6 / 99.9	96.2 / 99.1	90.0 / 92.1	74.2 / 75.8	<u>90.6</u> / 93.1
✓	✓	✓	✓	96.6 / 98.8	98.8 / 100.0	96.4 / 99.3	90.6 / 93.6	77.9 / 82.0	92.1 / 94.1

TABLE VII: RSWAttention Validity Studies on the Five Datasets.

Attention	GANGen-Detection	DiffusionForensics	UniversalFakeDetect	GenImage	AIGIBench	mean Acc. / A.P.
WAttention	70.7 / 82.9	65.8 / 89.5	73.2 / 88.4	71.5 / 81.2	58.3 / 63.2	67.9 / 81.0
RSWAttention	96.6 / 98.8	98.8 / 100.0	96.4 / 99.3	90.6 / 93.6	77.9 / 82.0	92.1 / 94.1

detection methods NPR and Ladedu, our method improves mean Acc. by 3.0% and 3.7%, respectively. However, methods Fatformer, C2P_CLIP, and AIDE, which have good results on other datasets, have an accuracy rate of less than 90% on this dataset, and even C2P_CLIP has only 80.7% accuracy. The most direct speculation for this result is that they used CLIP in the network skeleton, but the real reason is still worth further exploration. Additionally, on the UniversalFakeDetect dataset [43], our method achieves an average accuracy of 96.4%, 2.2% accuracy improvement over the best method.

GenImage [48]. Compared with testing only on diffusion or GAN, GenImage not only includes the classic GAN generation method, but also adds new and more realistic diffusion generation datasets, such as DALLE2. The test results are shown in Table IV. Our method achieves a notable improvement in mean accuracy, outperforming C2P_CLIP and Ladedu by 2.4% and 4.0%, respectively, and reaching an accuracy of 90.6%.

AIGIBench [49]. AIGIBench proposes a more challenging forgery detection dataset to evaluate the performance of forgery detection models from different perspectives. The test results are shown in Table V, our detection has achieved good results. Specifically, it achieves mean Accuracy (Acc.) and mean Average Precision (A.P.) of 77.9% and 82.0%, respectively. Compared to Ladedu and C2P_CLIP, our method improves mean Acc. by 3.0% and 5.9%, respectively. Although our results are the best, there are still major problems and improvements: 1) Although our method has achieved an accuracy rate of more than 90% in most GAN and diffusion scenarios, it still has an accuracy rate of only about 60% in the dataset collected in unknown generated social scenarios. Other methods also have very low accuracy rates, which still needs further research and improvement. 2) When it comes to face-swapping forgery detection, the performance is generally low, even less than 50%. Almost all methods have this problem, which is also a problem that needs to be considered and improved.

D. Qualitative Analysis

To further assess the generalization ability of our method, we visualize the logit distributions of NPR and our approach,

as shown in Figure 4. This visualization highlights how effectively each trained model distinguishes between real and fake images, showcasing our method’s ability to generalize across diverse fake representations. From the visualization, it is evident that NPR struggles with unseen GAN or diffusion models, showing significant overlap between the logits of real and fake categories, often misclassifying fake images as “real.” In contrast, our method demonstrates superior discrimination, effectively separating “real” and “fake” categories, even when encountering unseen sources.

E. Module Ablation Studies.

In order to comprehensively evaluate the effectiveness of our method, we conduct ablation studies on each module. The results of these experiments, shown in Table VI, demonstrate the contribution of each module to AI-generated image detection. Specifically, the experiment can prove that:

FFT alone has negative impacts on Attention. When we remove our main module (DWT-Based Window Tiling), the performance of our method drops significantly, falling below 50%. In our design, FFT is integrated as a parallel branch to complement DWT, leveraging its phase information to capture long-range dependencies that enhance fine-grained feature richness for reconstructed sliding window attention. However, the localized focus of RSWAttention, optimized for fine-grained details, appears incompatible with FFT’s global frequency representation when not moderated by DWT’s multi-scale decomposition or Window Tiling’s spatial structuring. This misalignment suggests that FFT alone introduces overly coarse features, diluting the attention mechanism’s ability to discern subtle, localized artifacts critical for deepfake identification.

Reasonable design of sliding window greatly improves the ability of attention extraction artifacts. Whether it is DWT or window tiling, the lack of any part will lead to a decrease in model accuracy. Without DWT, window attention cannot capture fine-grained artifacts. Removing Window Tiling yields a mean Acc. / A.P. of 90.3% / 93.4%, a notable decline from the full model’s 92.1% / 94.1%, suggesting that Window Tiling preserves critical spatial relationships within

TABLE VIII: Phase-only Part of FFT Validity Studies on the Five Datasets.

FFT		GANGen-Detection	DiffusionForensics	UniversalFakeDetect	GenImage	AIGIBench	mean Acc. / A.P.
Phase	Amp						
\times	\times	95.2 / 97.1	96.9 / 100.0	95.0 / 97.4	88.7 / 92.5	75.5 / 79.8	90.3 / 93.4
\checkmark	\times	96.6 / 98.8	98.8 / 100.0	96.4 / 99.3	90.6 / 93.6	77.9 / 82.0	92.1 / 94.1
\checkmark	\checkmark	93.0 / 97.0	91.3 / 99.2	92.2 / 97.2	85.1 / 91.2	72.7 / 77.8	86.9 / 92.5

TABLE IX: DWT Different Frequency Domain Subbands Studies on the Five Datasets.

DWT	GANGen-Detection	DiffusionForensics	UniversalFakeDetect	GenImage	AIGIBench	mean Acc. / A.P.
LL	65.7 / 79.9	63.6 / 84.7	68.5 / 82.2	66.0 / 78.0	57.3 / 62.3	64.2 / 77.4
LH	75.9 / 89.3	68.3 / 87.0	74.3 / 89.1	70.4 / 82.3	60.2 / 66.0	69.8 / 82.7
HL	78.9 / 88.3	69.7 / 86.2	74.5 / 85.6	71.8 / 82.7	61.7 / 66.2	71.3 / 81.8
HH	77.3 / 88.7	67.2 / 87.2	74.6 / 85.9	71.9 / 84.6	61.5 / 67.7	70.5 / 82.8
HL,HH	91.8 / 96.3	81.4 / 99.3	91.6 / 97.7	81.4 / 90.3	71.5 / 76.7	80.3 / 88.0
LH,HL,HH	90.7 / 98.0	84.0 / 99.9	92.5 / 99.0	84.3 / 93.0	73.8 / 80.5	85.1 / 94.0
LL,LH,HL,HH	96.6 / 98.8	98.8 / 100.0	96.4 / 99.3	90.6 / 93.6	77.9 / 82.0	92.1 / 94.1

TABLE X: Hyperparameter λ Ablation Experiment on the Five Datasets.

λ	GANGen-Detection	DiffusionForensics	UniversalFakeDetect	GenImage	AIGIBench	mean Acc.	mean A.P.
0.0	95.2 / 97.1	96.9 / 100.0	95.0 / 97.4	88.7 / 92.5	75.5 / 79.8	90.3	93.4
0.1	95.7 / 98.9	97.2 / 100.0	95.8 / 99.0	89.4 / 93.0	77.0 / 81.1	91.0	94.4
0.2	96.2 / 98.8	97.5 / 100.0	95.3 / 98.9	90.0 / 93.2	77.0 / 81.6	91.2	94.5
0.4	96.6 / 98.8	98.8 / 100.0	96.4 / 99.3	90.6 / 93.6	77.9 / 82.0	92.1	94.7
0.6	95.5 / 98.9	98.5 / 99.9	96.0 / 99.0	89.9 / 93.1	76.9 / 80.9	91.1	94.4
0.8	95.0 / 97.8	93.4 / 100.0	93.7 / 98.5	89.9 / 94.2	76.5 / 80.2	89.7	94.1
1.0	49.6 / 49.6	48.6 / 48.6	47.9 / 47.9	49.4 / 49.4	49.6 / 49.6	49.0	49.0

local windows, allowing RSWAttention to exploit Dependencies between local features. Without it, the disruption of these relationships impairs the model’s ability to detect localized artifacts, which is very important in datasets with complex or subtle manipulations. Therefore, carefully designed in-window features based on DWT and window tiling are crucial for RSWAttention to extract fine-grained forgery features.

It is effective to use the phase part of FFT as another branch. As shown in Table VI, when the phase part of FFT is excluded, the average accuracy of the model decreases 1.8%, indicating that FFT enhances the attention mechanism’s capacity to model interdependencies between distant image regions. FFT, as another frequency domain branch, enriches the local features within the window attention from different perspectives.

F. Comparative Studies of Module Design

To further verify that our proposed method helps the model extract more fine-grained multi-angle comprehensive forgery

traces while modeling the importance and implicit dependencies between local features, we conducted further comparative studies on the modules, as follows.

1) **The reconstructed sliding window attention mechanism greatly improves the ability of attention to capture forgery features.** As shown in Table VII, compared with WAttention, our RSWAttention improves the mean Acc. and mean A.P. by 24.2% and 13.1% respectively, which suggests that the RSWAttention greatly promotes the attention mechanism to capture fine-grained forgery traces within the local window while modeling the importance and interdependence between local features.

2) **Utilizing only the phase component of the FFT can reduce features not related to forgery compared to using the full FFT.** As shown in Table VIII, if we use not only the phase part of the FFT but also the amplitude part as input to the network, the average accuracy of the model drops by 5.2%, confirming that amplitude introduces noise or irrelevant intensity information that confounds the detector. In contrast, the phase, encoding structural details like edges and shapes,

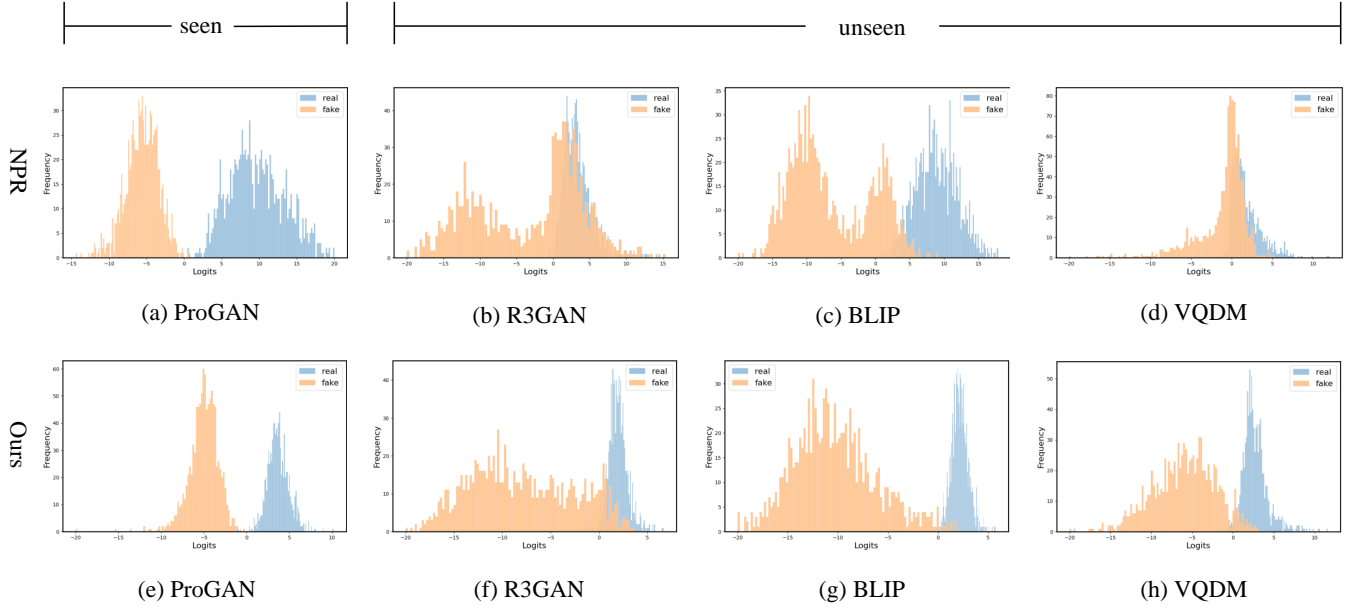


Fig. 4: **Logit Distributions of Extracted Forgery Features.** We compare the state of the art NRP [3] and our method, both tuned with 4-class ProGAN [19] data. A total of four testing GANs and diffusion models are considered, including ProGAN [19], R3GAN [58], BLIP [30] and VQDM [54], each randomly sampled 1k real and 1k fake images.

aligns with the artifact-relevant features needed for detection. This finding corroborates prior image processing research, where phase information is prioritized over amplitude for structural analysis, reinforcing our design choice to leverage FFT’s phase as a complementary input branch.

3) **All subbands of DWT are indispensable.** Each frequency domain subband of DWT has its own unique meaning, the low-frequency part retains the overall structure and semantic background of the image, and the high-frequency part captures subtle texture and edge information. Deleting any subband will reduce the comprehensiveness of the information in the window. As shown in Table IX, whether using only one frequency domain subband or omitting some frequency domain subbands, the performance of the model will be degraded.

G. Hyperparameter λ Ablation Study.

In order to more comprehensively evaluate the effectiveness of our method, we also conduct ablation experiments on the hyperparameter λ , which can be shown in Table X. When our parameter λ is set to 0.4 as set in the paper, the best results are achieved on all datasets.

V. CONCLUSION

In this paper, we propose a novel and effective method for AI-generated image detection. Specifically, we designed a reconstructed sliding window attention mechanism, which reconstructs the features within the window and limits the attention to the local window, forcing the attention to extract fine-grained features while modeling the importance and dependencies between internal elements in the local area. In addition, we design a dual frequency branch framework consisting of four frequency bands in the DWT domain and

the phase part in the FFT domain to extract richer local artifact features from multiple perspectives. Extensive experiments on 65 diverse generative models strongly demonstrate the generalization capability of our method.

REFERENCES

- [1] Yang Yu, Rongrong Ni, and Yao Zhao. Mining generalized features for detecting ai-manipulated fake faces. *arXiv preprint arXiv:2010.14129*, 2020.
- [2] Zhengzhe Liu, Xiaojuan Qi, and Philip HS Torr. Global texture enhancement for fake face detection in the wild. In *Proceedings of the IEEE/CVF conference on computer vision and pattern recognition*, pages 8060–8069, 2020.
- [3] Chuangchuang Tan, Yao Zhao, Shikui Wei, Guanghua Gu, Ping Liu, and Yunchao Wei. Rethinking the up-sampling operations in cnn-based generative network for generalizable deepfake detection. In *Proceedings of the IEEE/CVF Conference on Computer Vision and Pattern Recognition*, pages 28130–28139, 2024.
- [4] Shen Chen, Taiping Yao, Yang Chen, Shouhong Ding, Jilin Li, and Rongrong Ji. Local relation learning for face forgery detection. In *Proceedings of the AAAI conference on artificial intelligence*, volume 35, pages 1081–1088, 2021.
- [5] Lorenzo Baraldi, Federico Cocchi, Marcella Cornia, Alessandro Nicolosi, and Rita Cucchiara. Contrasting deepfakes diffusion via contrastive learning and global-local similarities. In *European Conference on Computer Vision*, pages 199–216. Springer, 2025.
- [6] Chende Zheng, Chenhao Lin, Zhengyu Zhao, Hang Wang, Xu Guo, Shuai Liu, and Chao Shen. Breaking semantic artifacts for generalized ai-generated image

- detection. *Advances in Neural Information Processing Systems*, 37:59570–59596, 2024.
- [7] Yonghyun Jeong, Doyeon Kim, Youngmin Ro, and Jongwon Choi. Frepgan: robust deepfake detection using frequency-level perturbations. In *Proceedings of the AAAI conference on artificial intelligence*, volume 36, pages 1060–1068, 2022.
- [8] Chuangchuang Tan, Yao Zhao, Shikui Wei, Guanghua Gu, and Yunchao Wei. Learning on gradients: Generalized artifacts representation for gan-generated images detection. In *Proceedings of the IEEE/CVF Conference on Computer Vision and Pattern Recognition*, pages 12105–12114, 2023.
- [9] Chuangchuang Tan, Yao Zhao, Shikui Wei, Guanghua Gu, Ping Liu, and Yunchao Wei. Frequency-aware deepfake detection: Improving generalizability through frequency space domain learning. In *Proceedings of the AAAI Conference on Artificial Intelligence*, volume 38, pages 5052–5060, 2024.
- [10] Kelvin Xu, Jimmy Ba, Ryan Kiros, Kyunghyun Cho, Aaron Courville, Ruslan Salakhudinov, Rich Zemel, and Yoshua Bengio. Show, attend and tell: Neural image caption generation with visual attention. In *International conference on machine learning*, pages 2048–2057. PMLR, 2015.
- [11] Ashish Vaswani, Noam Shazeer, Niki Parmar, Jakob Uszkoreit, Llion Jones, Aidan N Gomez, Łukasz Kaiser, and Illia Polosukhin. Attention is all you need. *Advances in neural information processing systems*, 30, 2017.
- [12] Alexey Dosovitskiy, Lucas Beyer, Alexander Kolesnikov, Dirk Weissenborn, Xiaohua Zhai, Thomas Unterthiner, Mostafa Dehghani, Matthias Minderer, Georg Heigold, Sylvain Gelly, et al. An image is worth 16x16 words: Transformers for image recognition at scale. *arXiv preprint arXiv:2010.11929*, 2020.
- [13] Supriyo Sadhya and Xiaojun Qi. Deepfake detection with wavelet-integrated convolutional networks. In *2024 IEEE International Conference on Big Data (BigData)*, pages 4540–4547. IEEE, 2024.
- [14] Nour Eldin Alaa Badr, Jean-Christophe Nebel, Darrel Greenhill, and Xing Liang. Wavit-cdc: wavelet vision transformer with central difference convolutions for spatial-frequency deepfake detection. *IEEE Open Journal of Signal Processing*, 2025.
- [15] Huan Liu, Zichang Tan, Chuangchuang Tan, Yunchao Wei, Jingdong Wang, and Yao Zhao. Forgery-aware adaptive transformer for generalizable synthetic image detection. In *Proceedings of the IEEE/CVF Conference on Computer Vision and Pattern Recognition*, pages 10770–10780, 2024.
- [16] Chen Zhao, Weiling Cai, Chenyu Dong, and Chengwei Hu. Wavelet-based fourier information interaction with frequency diffusion adjustment for underwater image restoration. In *Proceedings of the IEEE/CVF Conference on Computer Vision and Pattern Recognition*, pages 8281–8291, 2024.
- [17] Chuangchuang Tan, Renshuai Tao, Huan Liu, Guanghua Gu, Baoyuan Wu, Yao Zhao, and Yunchao Wei. C2p-clip: Injecting category common prompt in clip to enhance generalization in deepfake detection. In *Proceedings of the AAAI Conference on Artificial Intelligence*, volume 39, pages 7184–7192, 2025.
- [18] Shilin Yan, Ouxiang Li, Jiayin Cai, Yanbin Hao, Xiaolong Jiang, Yao Hu, and Weidi Xie. A sanity check for ai-generated image detection. *arXiv preprint arXiv:2406.19435*, 2024.
- [19] Tero Karras. Progressive growing of gans for improved quality, stability, and variation. *arXiv preprint arXiv:1710.10196*, 2017.
- [20] Andrew Brock. Large scale gan training for high fidelity natural image synthesis. *arXiv preprint arXiv:1809.11096*, 2018.
- [21] Yunje Choi, Minje Choi, Munyoung Kim, Jung-Woo Ha, Sunghun Kim, and Jaegul Choo. Stargan: Unified generative adversarial networks for multi-domain image-to-image translation. In *Proceedings of the IEEE conference on computer vision and pattern recognition*, pages 8789–8797, 2018.
- [22] Andreas Rossler, Davide Cozzolino, Luisa Verdoliva, Christian Riess, Justus Thies, and Matthias Nießner. Faceforensics++: Learning to detect manipulated facial images. In *Proceedings of the IEEE/CVF international conference on computer vision*, pages 1–11, 2019.
- [23] Prafulla Dhariwal and Alexander Nichol. Diffusion models beat gans on image synthesis. *Advances in neural information processing systems*, 34:8780–8794, 2021.
- [24] Robin Rombach, Andreas Blattmann, Dominik Lorenz, Patrick Esser, and Björn Ommer. High-resolution image synthesis with latent diffusion models. In *Proceedings of the IEEE/CVF conference on computer vision and pattern recognition*, pages 10684–10695, 2022.
- [25] Midjourney Team. Midjourney v6.1. <https://www.midjourney.com/home>. 2024.
- [26] Black Forest Labs. Flux.1-dev. <https://huggingface.co/black-forest-labs/FLUX.1-dev>. 2024.
- [27] Qixun Wang, Xu Bai, Haofan Wang, Zekui Qin, Anthony Chen, Huaxia Li, Xu Tang, and Yao Hu. Instantid: Zero-shot identity-preserving generation in seconds. *arXiv preprint arXiv:2401.07519*, 2024.
- [28] Yi Wu, Ziqiang Li, Heliang Zheng, Chaoyue Wang, and Bin Li. Infinite-id: Identity-preserved personalization via id-semantics decoupling paradigm. In *European Conference on Computer Vision*, pages 279–296. Springer, 2024.
- [29] Zhen Li, Mingdeng Cao, Xintao Wang, Zhongang Qi, Ming-Ming Cheng, and Ying Shan. Photomaker: Customizing realistic human photos via stacked id embedding. In *Proceedings of the IEEE/CVF conference on computer vision and pattern recognition*, pages 8640–8650, 2024.
- [30] Junnan Li, Dongxu Li, Caiming Xiong, and Steven Hoi. Blip: Bootstrapping language-image pre-training for unified vision-language understanding and generation. In *International conference on machine learning*, pages 12888–12900. PMLR, 2022.
- [31] Hu Ye, Jun Zhang, Sibao Liu, Xiao Han, and Wei

- Yang. Ip-adapter: Text compatible image prompt adapter for text-to-image diffusion models. *arXiv preprint arXiv:2308.06721*, 2023.
- [32] Alexandros Haliassos, Konstantinos Vougioukas, Stavros Petridis, and Maja Pantic. Lips don't lie: A generalisable and robust approach to face forgery detection. In *Proceedings of the IEEE/CVF conference on computer vision and pattern recognition*, pages 5039–5049, 2021.
- [33] Liang Chen, Yong Zhang, Yibing Song, Lingqiao Liu, and Jue Wang. Self-supervised learning of adversarial example: Towards good generalizations for deepfake detection. In *Proceedings of the IEEE/CVF conference on computer vision and pattern recognition*, pages 18710–18719, 2022.
- [34] Lucy Chai, David Bau, Ser-Nam Lim, and Phillip Isola. What makes fake images detectable? understanding properties that generalize. In *Computer Vision—ECCV 2020: 16th European Conference, Glasgow, UK, August 23–28, 2020, Proceedings, Part XXVI 16*, pages 103–120. Springer, 2020.
- [35] Bar Cavia, Eliahu Horwitz, Tal Reiss, and Yedid Hoshen. Real-time deepfake detection in the real-world. *arXiv preprint arXiv:2406.09398*, 2024.
- [36] Zehao Chen and Hua Yang. Manipulated face detector: Joint spatial and frequency domain attention network. *arXiv preprint arXiv:2005.02958*, 1(2):4, 2020.
- [37] Yuyang Qian, Guojun Yin, Lu Sheng, Zixuan Chen, and Jing Shao. Thinking in frequency: Face forgery detection by mining frequency-aware clues. In *European conference on computer vision*, pages 86–103. Springer, 2020.
- [38] Joel Frank, Thorsten Eisenhofer, Lea Schönherr, Asja Fischer, Dorothea Kolossa, and Thorsten Holz. Leveraging frequency analysis for deep fake image recognition. In *International conference on machine learning*, pages 3247–3258. PMLR, 2020.
- [39] Yuchen Luo, Yong Zhang, Junchi Yan, and Wei Liu. Generalizing face forgery detection with high-frequency features. In *Proceedings of the IEEE/CVF conference on computer vision and pattern recognition*, pages 16317–16326, 2021.
- [40] Hanqing Zhao, Wenbo Zhou, Dongdong Chen, Tianyi Wei, Weiming Zhang, and Nenghai Yu. Multi-attentional deepfake detection. In *Proceedings of the IEEE/CVF conference on computer vision and pattern recognition*, pages 2185–2194, 2021.
- [41] Jiahui Wu, Yu Zhu, Xiaoben Jiang, Yatong Liu, and Jiajun Lin. Local attention and long-distance interaction of rppg for deepfake detection. *The Visual Computer*, 40(2):1083–1094, 2024.
- [42] Alec Radford, Jong Wook Kim, Chris Hallacy, Aditya Ramesh, Gabriel Goh, Sandhini Agarwal, Girish Sastry, Amanda Askell, Pamela Mishkin, Jack Clark, et al. Learning transferable visual models from natural language supervision. In *International conference on machine learning*, pages 8748–8763. PmLR, 2021.
- [43] Utkarsh Ojha, Yuheng Li, and Yong Jae Lee. Towards universal fake image detectors that generalize across generative models. In *Proceedings of the IEEE/CVF Conference on Computer Vision and Pattern Recognition*, pages 24480–24489, 2023.
- [44] Haiwei Wu, Jiantao Zhou, and Shile Zhang. Generalizable synthetic image detection via language-guided contrastive learning. *arXiv preprint arXiv:2305.13800*, 2023.
- [45] Zihan Liu, Hanyi Wang, Yaoyu Kang, and Shilin Wang. Mixture of low-rank experts for transferable ai-generated image detection. *arXiv preprint arXiv:2404.04883*, 2024.
- [46] Zhendong Wang, Jianmin Bao, Wengang Zhou, Weilun Wang, Hezhen Hu, Hong Chen, and Houqiang Li. Dire for diffusion-generated image detection. In *Proceedings of the IEEE/CVF International Conference on Computer Vision*, pages 22445–22455, 2023.
- [47] Jimmy Lei Ba, Jamie Ryan Kiros, and Geoffrey E Hinton. Layer normalization. *ArXiv e-prints*, pages arXiv–1607, 2016.
- [48] Mingjian Zhu, Hanting Chen, Qiangyu Yan, Xudong Huang, Guanyu Lin, Wei Li, Zhijun Tu, Hailin Hu, Jie Hu, and Yunhe Wang. Genimage: A million-scale benchmark for detecting ai-generated image. *Advances in Neural Information Processing Systems*, 36, 2024.
- [49] Ziqiang Li, Jiazhen Yan, Ziwen He, Kai Zeng, Weiwei Jiang, Lizhi Xiong, and Zhangjie Fu. Is artificial intelligence generated image detection a solved problem? *arXiv preprint arXiv:2505.12335*, 2025.
- [50] Sheng-Yu Wang, Oliver Wang, Richard Zhang, Andrew Owens, and Alexei A Efros. Cnn-generated images are surprisingly easy to spot... for now. In *Proceedings of the IEEE/CVF conference on computer vision and pattern recognition*, pages 8695–8704, 2020.
- [51] Jonathan Ho, Ajay Jain, and Pieter Abbeel. Denoising diffusion probabilistic models. *Advances in neural information processing systems*, 33:6840–6851, 2020.
- [52] Alexander Quinn Nichol and Prafulla Dhariwal. Improved denoising diffusion probabilistic models. In *International conference on machine learning*, pages 8162–8171. PMLR, 2021.
- [53] Luping Liu, Yi Ren, Zhijie Lin, and Zhou Zhao. Pseudo numerical methods for diffusion models on manifolds. *arXiv preprint arXiv:2202.09778*, 2022.
- [54] Shuyang Gu, Dong Chen, Jianmin Bao, Fang Wen, Bo Zhang, Dongdong Chen, Lu Yuan, and Baining Guo. Vector quantized diffusion model for text-to-image synthesis. In *Proceedings of the IEEE/CVF conference on computer vision and pattern recognition*, pages 10696–10706, 2022.
- [55] Aditya Ramesh, Mikhail Pavlov, Gabriel Goh, Scott Gray, Chelsea Voss, Alec Radford, Mark Chen, and Ilya Sutskever. Zero-shot text-to-image generation. In *International conference on machine learning*, pages 8821–8831. Pmlr, 2021.
- [56] Diederik P Kingma. Adam: A method for stochastic optimization. *arXiv preprint arXiv:1412.6980*, 2014.
- [57] Sara Mandelli, Nicolò Bonettini, Paolo Bestagini, and Stefano Tubaro. Detecting gan-generated images by orthogonal training of multiple cnns. In *2022 IEEE*

International Conference on Image Processing (ICIP), pages 3091–3095. IEEE, 2022.

- [58] Nick Huang, Aaron Gokaslan, Volodymyr Kuleshov, and James Tompkin. The gan is dead; long live the gan! a modern gan baseline. *Advances in Neural Information Processing Systems*, 37:44177–44215, 2024.